Appl Phys B (2012) 107:503–511
DOI 10.1007/s00340-012-4927-7

Applied Physics B
Lasers and Optics

Synthesis, characterization, thermo- and photoluminescence properties of Bi^{3+} co-doped $Gd_2O_3:Eu^{3+}$ nanophosphors

N. Dhananjaya · H. Nagabhushana · B.M. Nagabhushana · S.C. Sharma · B. Rudraswamy · N. Suriyamurthy · C. Shivakumara · R.P.S. Chakradhar

Received: 27 June 2011 / Published online: 6 April 2012

Abstract $Gd_2O_3:Eu^{3+}$ (4 mol%) co-doped with Bi^{3+} (Bi = 0, 1, 3, 5, 7, 9 and 11 mol%) ions were synthesized by a low-temperature solution combustion method. The powders were calcined at 800°C and were characterized by powder X-ray diffraction (PXRD), transmission electron microscopy (TEM), Fourier transform infrared and UV–Vis spectroscopy. The PXRD profiles confirm that the calcined products were in monoclinic with little cubic phases. The particle sizes were estimated using Scherrer's method and Williamson–Hall plots and are found to be in the ranges 40–60 nm and 30–80 nm, respectively. The results are in good agreement with TEM results. The photoluminescence spectra of the synthesized phosphors excited with 230 nm show emission peaks at ∼590, 612 and 625 nm, which are due to the transitions $^5D_0 \rightarrow {}^7F_0$, $^5D_0 \rightarrow {}^7F_2$ and $^5D_0 \rightarrow {}^7F_3$ of Eu^{3+}, respectively. It is observed that a significant quenching of Eu^{3+} emission was observed under 230 nm excitation when Bi^{3+} was co-doped. On the other hand, upon 350 nm excitation, the luminescent intensity of Eu^{3+} ions was enhanced by incorporation of Bi^{3+} (5 mol%) ions. The introduction of Bi^{3+} ions broadened the excitation band of Eu^{3+} of which a new strong band occurred ranging from 320 to 380 nm. This has been attributed to the $6s^2 \rightarrow 6s6p$ transition of Bi^{3+} ions, implying a very efficient energy transfer from Bi^{3+} ions to Eu^{3+} ions. The gamma radiation response of $Gd_2O_3:Eu^{3+}$ exhibited a dosimetrically useful glow peak at 380°C. Using thermoluminescence glow peaks, the trap parameters have been evaluated and discussed. The observed emission characteristics and energy transfer indicate that $Gd_2O_3:Eu^{3+}$, Bi^{3+} phosphors have promising applications in solid-state lighting.

N. Dhananjaya · B. Rudraswamy
Department of Physics, J.B. Campus, Bangalore University, Bangalore 560 056, India

B. Rudraswamy
e-mail: brudraswamy@gmail.com

N. Dhananjaya
Department of Physics, B.M.S. Institute of Technology, Bangalore 560 064, India

H. Nagabhushana (✉) · S.C. Sharma
Prof. C.N.R. Rao Centre for Nano Research (CNR), Tumkur University, Tumkur 572 103, India
e-mail: bhushanvlc@gmail.com

B.M. Nagabhushana
Department of Chemistry, M.S. Ramaiah Institute of Technology, Bangalore 560 054, India

N. Suriyamurthy
Indira Gandhi Centre for Atomic Research (IGCAR), Kalpakam 603 102, India

C. Shivakumara
Solid State and Structural Chemistry Unit, Indian Institute of Science, Bangalore 560 012, India

R.P.S. Chakradhar (✉)
National Aerospace Laboratories (CSIR), Bangalore 560 017, India
e-mail: sreechakra72@yahoo.com

1 Introduction

Rare-earth (RE) sesquioxides doped with lanthanide active ions have been widely used for various applications such as solid-state lasers, luminescent lamps, flat display, phosphor display panels (PDPs), field emission displays (FEDs), light-emitting diodes (LEDs) and photonic devices [1–5]. Among RE sesquioxides, Gd_2O_3 is a promising host matrix for rare-earth ions due to its good thermal stability and chemical durability [6, 7]. Gd_2O_3 doped with trivalent Eu has attracted much attention as a dopant because of its intense red emission at 611 nm under UV excitation and proved to be an excellent red-emission phosphor [8]. The enhancement of emission intensity is very important for research and application of luminescent materials. Therefore, in recent times many researchers started working on the enhancement of luminescence efficiency of these phosphors by activating them by co-doping with either rare-earth or transition-metal ions in different host matrices [9–12]. Transition-metal (TM) ions generally have larger oscillator strengths than rare-earth ions and can therefore absorb more of the input energy. On the other hand, using rare-earth ions has certain advantages; first, because of their simple and well-defined luminescence scheme, they serve as a very efficient and sensitive structural probe and secondly, their luminescence in the case of a non-centrosymmetric environment is generally dominated by the $^5D_0 \rightarrow {}^7F_2$ transition yielding a red emission which is suitable for display applications.

Low-temperature chemical methods have been proven to be very useful means for determining the properties of a variety of functional nanomaterials over the last few decades [13–17]. As a part of our programme on nanophosphors, here we report the tunable luminescent properties of Gd_2O_3:Eu^{3+} co-doped with Bi^{3+} ions prepared by a low-temperature solution combustion method. Based on an extensive literature survey, it has been found that little work has been reported on the luminescent properties of Bi^{3+} co-doped with Eu^{3+} activators and energy transfer between Bi^{3+} and Eu^{3+} ions. The Bi^{3+} ion with outer $6S^2$ configuration is of large importance as an activator in the field of luminescence [18]. The Bi^{3+} ion shows a ground state $^1S_0$ and excited states $^3P_0$, $^3P_1$, $^3P_2$ and $^1P_1$ (in sequence of increasing energy). The transitions from $^1S_0$ to $^3P_0$ and $^3P_2$ are completely spin forbidden, while the two levels $^3P_1$ and $^1P_1$ are mixed by spin–orbit coupling. Therefore, only the transitions $^1S_0 \rightarrow {}^3P_1$ and $^1P_1$ are expected to have reasonable absorption strength [19]. Co-doped with Bi^{3+} ions, the excitation efficiency of Eu^{3+} in the UV range can be enormously enhanced by the energy transfer from the Bi^{3+} ions to the Eu^{3+} ions.

This paper mainly focuses on the synthesis and luminescent properties of Gd_2O_3:Eu^{3+} (4 mol%), Bi^{3+} (0–11 mol%) nanophosphors and the study of energy transfer between Bi^{3+} and Eu^{3+} ions. The synthesized phosphors are well characterized by using powder X-ray diffraction (PXRD), transmission electron microscopy (TEM), Fourier transform infrared (FTIR) and UV–Vis spectroscopy. In addition, we report the photo- and thermoluminescent properties of the nanophosphors. The thermoluminescence (TL) method is generally used to study defects in insulators and semiconductors. Moreover, this method has been successfully applied in the field of radiation dosimetry [20]. Many synthetic materials especially oxide materials have been developed and characterized to evaluate their feasibility as TL dosimeters [21]. However, there is less work on TL properties of Bi^{3+} co-doped to Gd_2O_3:Eu^{3+} nanophosphors reported so far.

2 Experimental

2.1 Synthesis of Bi^{3+} co-doped Gd_2O_3:Eu^{3+} nanophosphors

In typical synthesis of Gd_2O_3:Eu^{3+} (4 mol%), Bi^{3+} (Bi = 0, 1, 3, 5, 7, 9 and 11 mol%) nanophosphors, gadolinium nitrate [$Gd(NO_3)_3$], europium nitrate [$Eu(NO_3)_3$], bismuth nitrate [$Bi(NO_3)_3$] and oxalyl dihydrazide [ODH: $C_2H_6N_4O_2$] were weighed at a stoichiometric ratio and dissolved in double-distilled water. The resulting mixture was transferred into a petri dish and then introduced into a muffle furnace maintained at 400 ± 10°C. The mixture undergoes dehydrations and then decomposes with liberation of large amounts of gases (CO_2 and N_2). The mixture was then frothed and swelled thus forming foam which ruptured with a flame and glowed to incandescence. During incandescence, the foam further swelled to the capacity of the container. The whole combustion process was over in less than a few minutes (<5 min). The petri dish was taken out from the furnace and a foamy product was crushed into fine powder using a pestle and mortar. These powders were calcined at 800°C for 3 h, and their thermo- and photoluminescence properties were investigated.

2.2 Instruments used

The phase purity and the crystallinity of the nanophosphors was examined by a powder X-ray diffractometer (PANalytical X′Pert Pro) using CuK_α (1.541 Å) radiation with a nickel filter. Transmission electron microscopy (TEM) analysis was performed on a Hitachi H-8100 (accelerating voltage up to 200 kV, LaB_6 filament) microscope. The FTIR studies have been performed on a Perkin Elmer spectrometer (Spectrum 1000) with KBr pellets. The UV–Vis absorption of the samples was recorded on a SL 159 ELICO UV–Vis spectrophotometer. The photoluminescence (PL) measurements were performed on a Jobin Yvon spectrofluorimeter (Fluorolog–3) equipped with a 450-W xenon lamp as an excitation source. TL measurements were carried out at room temperature using a Nucleonix TL reader using a ^{60}Co gamma source as excitation in the dose 1 kGy.

3 Results and discussion

The powder X-ray diffraction (PXRD) patterns of synthesized Gd_2O_3:Eu^{3+} (4 mol%), Bi^{3+} (Bi = 0, 1, 3, 5, 7, 9 and

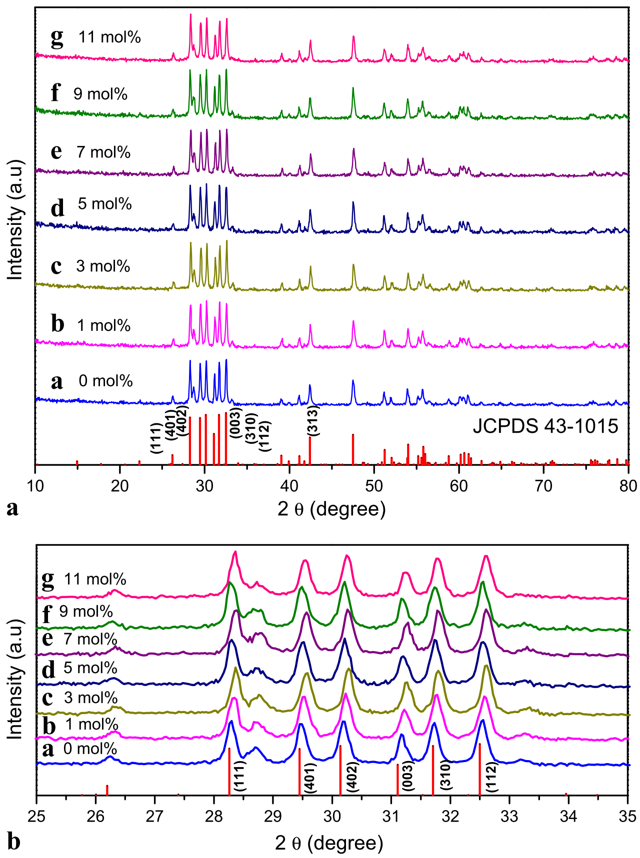

Fig. 1 (**a**) Powder X-ray diffraction patterns of $Gd_2O_3:Eu^{3+}$, Bi^{3+} (0–11 mol%) nanophosphors calcined at 800°C for 3 h. (**b**) Magnified view of 2θ values from 25 to 35 degrees

11 mol%) nanophosphors are shown in Fig. 1a. All of the diffracted peaks are corresponding to a monoclinic phase of Gd_2O_3 (JCPDS no. 43-1015) with little cubic phase of Gd_2O_3 [15]. No impurity peaks were observed, indicating that Eu^{3+} and Bi^{3+} ions have occupied the Gd^{3+} sites completely. However, a small peak shift was observed when Gd^{3+} ions are substituted by a larger Bi^{3+} ion concentration (Fig. 1b). There are various factors which affect the broadening of diffraction peaks, namely (i) crystalline domain size, (ii) domain size distribution, (iii) crystalline facets (external defects) and microstrain (deformation of the lattice), etc. The crystallite size (d) was estimated from the broad PXRD peaks using Scherrer's method [22]:

$$d = \frac{0.9\lambda}{\beta\cos\theta}, \tag{1}$$

where d is the average grain size of the crystallites, λ is the wavelength of the CuK_α (1.541 Å) radiation, θ is the angle between the incident beam and the reflection lattice planes and β is the full width at half maximum (FWHM) of the diffraction peak in radians. The average crystalline domain size of the nanoparticles was found to be in the range 40–60 nm. Further, the broadening of PXRD peaks is due

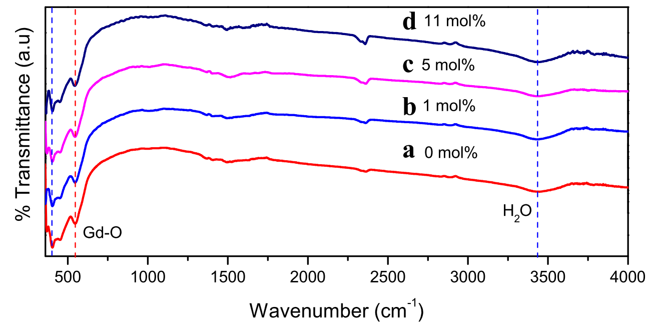

Fig. 2 FTIR spectra of $Gd_2O_3:Eu^{3+}$, Bi^{3+} (0–11 mol%) nanophosphors calcined at 800°C for 3 h

to microstrain, which is proportional to $\tan\theta$. Thus, we can obtain the Williamson–Hall formula [23] by combining the effect on powder X-ray diffraction patterns for broadening:

$$\frac{\beta\cos\theta}{\lambda} = \frac{0.9}{D} + \frac{\varepsilon\sin\theta}{\lambda}, \tag{2}$$

where ε measures the microstrain value.

The plot of $\beta\cos\theta/\lambda$ versus $\sin\theta/\lambda$ is a linear fit. The slope of the graph gives the amount of microstrain and the intercept on the $\beta\cos\theta/\lambda$ axis gives the crystallite size. The estimated microstrain was observed to be in the range 5–13 $\times 10^{-3}$.

Figure 2 depicts the typical FTIR spectra of 0, 1, 5 and 11 mol% Bi co-doped $Gd_2O_3:Eu^{3+}$ nanophosphor. It is found that the small absorption peak at 3410 cm^{-1} is due to adsorbed water and the CO_3^{2-} anion groups were observed at 1374 and 1586 cm^{-1}. We believe that the possible source of the carbonyl group is from oxalyl dihydrazide fuel. The strong absorption peak near 540 cm^{-1} is associated with the vibration of the Gd–O bond [24].

Figure 3a shows the typical TEM image of the Gd_2O_3: Eu^{3+}, Bi^{3+} (1 mol%) nanophosphors. The nanocrystals were dispersed in acetone and a drop of the dispersion was deposited on a copper grid covered by a holey carbon film (HD 200 copper Formvar/carbon). The particles are spherical in shape with varying sizes ranging from 40 to 60 nm and the results are in good agreement with those obtained from Scherrer's method and Williamson–Hall studies. The selected area electron diffraction (SAED) pattern of the nanocrystals is shown in Fig. 3b and the corresponding energy-dispersive X-ray (EDX) spectrum is given in Fig. 3c.

UV–Vis absorption spectra of $Gd_2O_3:Eu^{3+}$ (4 mol%) and $Gd_2O_3:Eu^{3+}$, Bi^{3+} (1 mol%) phosphors are shown in Fig. 4a. The samples of $Gd_2O_3:Eu^{3+}$ and Bi^{3+} co-doped show a strong absorption band in the region 300–550 nm, which is attributed to the excitation absorption of Bi^{3+} and Eu^{3+}, respectively [25]. The higher-energy bands at wavelengths shorter than 240 nm in the absorption spectra result from true fundamental absorption of the Gd_2O_3 host lattice. The small absorption peak at 275 nm is corresponding to

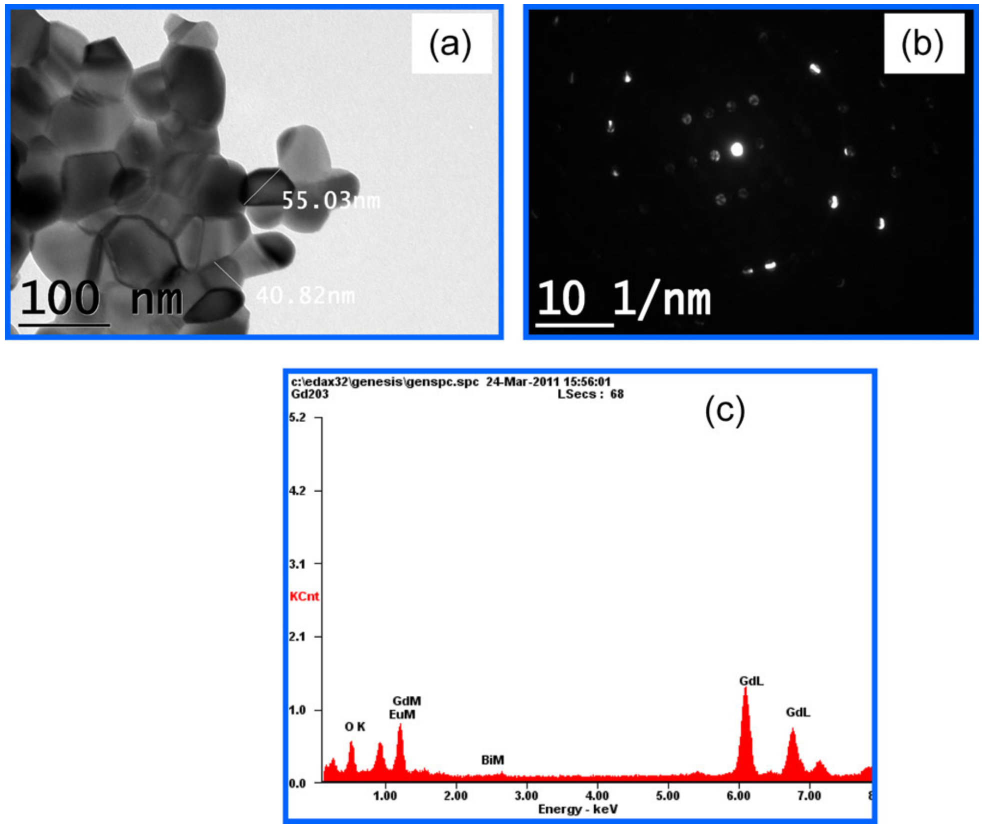

Fig. 3 (**a**) TEM image, (**b**) SAED pattern, (**c**) EDX image of Gd_2O_3:Eu^{3+}, Bi^{3+} (1 mol%) nanophosphors

the 4f–4f transition ($^8S_{7/2} \rightarrow {}^6I_J$) of Gd^{3+}. The absorption intensity from 240 to 420 nm is highly increased by the incorporation of Bi^{3+} ions (inset of Fig. 4a). The absorption band around 260, 340 and 370 nm is assigned to the excitation absorption of Bi^{3+} [26, 27]. The absorption band is found to be shifted towards the higher-wavelength side with increasing concentration of Bi^{3+}. This is due to the transition between the conduction band and the impurity level generated due to Bi^{3+} doping.

The optical band gap energy (E_g) is related to the absorption coefficient α by the Tauc relation [28]. According to the Tauc relation, the absorption coefficient α for a direct band gap is given by

$$\alpha h\upsilon \sim C_1 (h\upsilon - E_g)^{1/2} \tag{3}$$

where C_1 is the proportionality constant, which is different for different transitions. For an allowed direct transition an extrapolation of the linear region of a plot of $(\alpha h\upsilon)^2$ on the Y-axis versus photon energy ($h\upsilon$) on the X-axis gives the value of the optical band gap E_g. Figure 4b shows the plots of $(\alpha h\upsilon)^2$ versus $h\upsilon$ for the Gd_2O_3:Eu^{3+}, Bi^{3+} nanophosphor. It is observed that the energy band gap of the Gd_2O_3:Eu^{3+}, Bi^{3+} (1 mol%) nanophosphor is more when compared to Gd_2O_3:Eu^{3+}.

Figure 5 shows the photoluminescence excitation (PLE) spectra of Gd_2O_3:Eu^{3+}, Bi^{3+} (0–11 mol%) nanophosphors at room temperature. The band exciting from 220 to 300 nm is associated with an O^{2-}–Eu^{3+} charge-transfer (CT) transition. In addition to this, a broad band was observed in the range 300–380 nm due to the absorption of Bi^{3+} in the host. The excitation spectra consist of sharp lines ascribed to transitions of Eu^{3+}, $^7F_0 \rightarrow {}^5L_9$ (358 nm), $^5G_5$ (380 nm), $^5L_6$ (391 nm), $^5D_3$ (442 nm) and $^5D_2$ (462 nm). The enlarged view in the range 300–500 nm is shown in the inset of Fig. 5. Figure 6 shows the emission spectra of Gd_2O_3:Eu^{3+}, Bi^{3+} (0–11 mol%) nanophosphor upon 230 nm excitation. The intense peak observed at 612 nm is assigned to the $^5D_0 \rightarrow {}^7F_2$ transition of Eu^{3+} ions, and the peak around 588 nm is related to the $^5D_0 \rightarrow {}^7F_1$ transition. The emission peaks from $^5D_1 \rightarrow {}^7F_J$ ($J = 1, 2$) transitions were also detected in the range 525–570 nm. The variation of PL intensity in Gd_2O_3:Eu^{3+}, Bi^{3+} (0–11 mol%) nanophosphor with Bi^{3+} concentration is shown in Fig. 7. It is interesting to observe that upon 230 nm excitation the PL emission is more in without the Bi^{3+} co-doped Gd_2O_3:Eu^{3+} sample. Further, with increase of Bi^{3+} concentration the PL intensity is found to decrease.

Figure 8 shows the emission spectra of Gd_2O_3:Eu^{3+}, Bi^{3+} (0–11 mol%) nanophosphors when excited at 350 nm. It is observed that in the emission spectra, the band edge shifts to longer wavelengths with increasing Bi^{3+} concentration. This change is due to the extra absorption impurity Bi–O component in addition to Gd–O charge-transfer

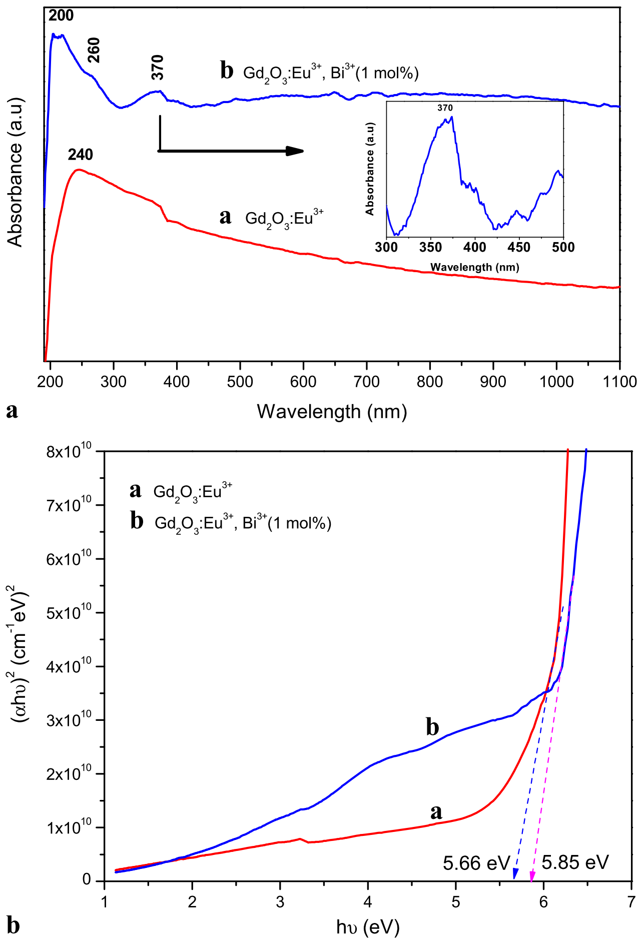

Fig. 4 (**a**) UV–Vis absorption spectra, (**b**) energy gaps of $Gd_2O_3:Eu^{3+}$ and $Gd_2O_3:Eu^{3+}$, Bi^{3+} (1 mol%) nanophosphors

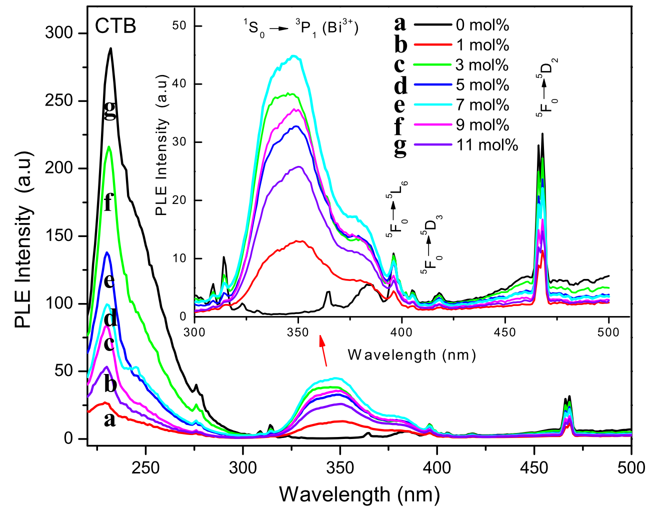

Fig. 5 Photoluminescence excitation (PLE) spectra of $Gd_2O_3:Eu^{3+}$, Bi^{3+} (0–11 mol%) nanophosphors calcined at 800°C for 3 h (*inset*: enlarged view of PLE spectra from 300 to 500 nm)

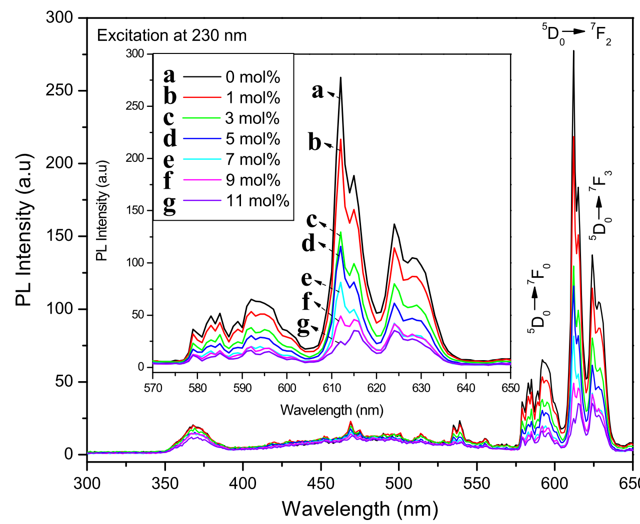

Fig. 6 PL spectra (excited at 230 nm) of $Gd_2O_3:Eu^{3+}$, Bi^{3+} (0–11 mol%) nanophosphors calcined at 800°C for 3 h (*inset*: enlarged view of PL spectra from 570 to 650 nm)

bands. This change seems to be significant only when the Bi^{3+} concentration was less than 5 mol%. For substitutions exceeding 5 mol% Bi^{3+}, the emission intensity of the long-wavelength band is diminished. The changes can be clearly visualized from the inset of Fig. 8. The variation of PL intensity as a function Bi^{3+} concentration (1–11 mol%) under 350 nm excitation wavelength is shown in Fig. 9. It is observed that the 5 mol% Bi^{3+} concentration was determined to be the best value for strongest Eu^{3+} emission. Above this value, the intensity of Eu^{3+} emission decreases with increase of Bi^{3+} concentration. The decrease of the emission intensity is due to the concentration quenching of Bi^{3+} ions. At higher doping concentrations, the distance between Bi^{3+} ions becomes shorter. The larger the concentration of Bi^{3+} ions, the shorter the distance between the Bi^{3+} ions is, the farther the distraction of the energy transfer along the Bi^{3+} ions will be, resulting in greater probability of transferring energy from Bi^{3+} ions to the quenching centres. So, there will be less energy transfer from Bi^{3+} ions to Eu^{3+} ions and the emission intensity decreases [17].

Figure 10a shows the variation of PL intensity under 230 and 350 nm excitation as a function of Bi^{3+} concentration. The emission spectra appear with the same features of $^5D_0 \rightarrow {}^7F_J$ ($J = 0$, 1, 2, 3 and 4) peaks except for different emission intensities. As we can see, the PL intensity is more upon 230 nm excitation when compared to 350 nm. This difference is due to the fact that the transition corresponding to 230 nm is from a completely allowed transition of CT and therefore at 230 nm excitation we observed high luminescence intensity compared to excitation at 350 nm. Further, the PL intensity ratios of the $^5D_0 \rightarrow {}^7F_1$ transition to $^5D_0 \rightarrow {}^7F_2$ at various Bi^{3+} concentrations are shown in Fig. 10b. It is found that the asymmetric ratio increases with

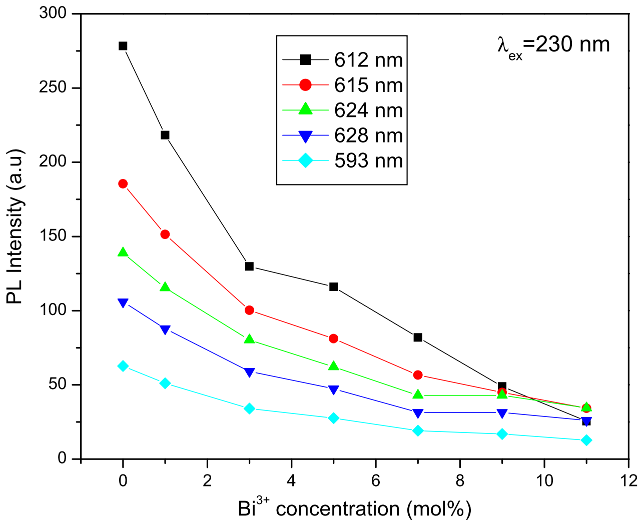

Fig. 7 Variation in PL intensity of different emission peaks versus Bi^{3+}concentration in $Gd_2O_3:Eu^{3+}$, Bi^{3+} (0–11 mol%) nanophosphors at 230 nm excitation wavelength

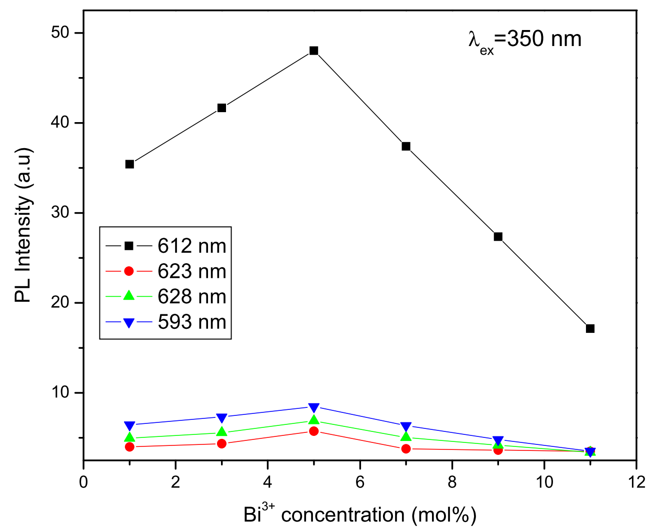

Fig. 9 Variation in PL intensity of different emission peaks versus Bi^{3+}concentration in $Gd_2O_3:Eu^{3+}$, Bi^{3+} (1–11 mol%) at 350 nm excitation wavelength

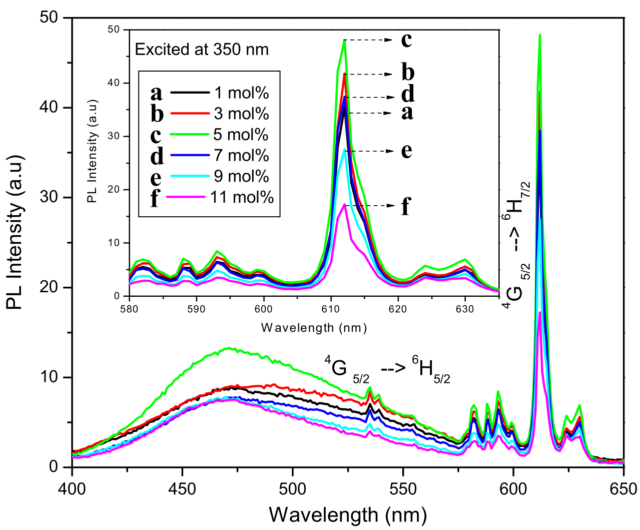

Fig. 8 PL spectra (excited at 350 nm) of $Gd_2O_3:Eu^{3+}$, Bi^{3+} (0–11 mol%) nanophosphors calcined at 800°C for 3 h

increasing of Bi^{3+} concentration. It is also found that the $^5D_0 \rightarrow {}^7F_2$ intensity of $Gd_2O_3:Eu^{3+}$, Bi^{3+} upon 350 nm excitation is close to the peak value of $Gd_2O_3:Eu^{3+}$ under 230 nm excitation, and it indicates that Bi^{3+} can act as efficient doping ions for the emission in the near-UV region. The reason is that the excitation spectra of Bi^{3+} and Eu^{3+} are overlapping, so the energy transfer occurs between them, which can be described as a Bi^{3+}–Gd^{3+}–Eu^{3+} system. So, we find that Bi^{3+} ions greatly enhance the luminescence intensities of $Gd_2O_3:Eu^{3+}$ nanophosphors and make these nanophosphors suitable red-emitting materials that can be pumped with near UV light emitting diodes (LEDs). The possible energy transfer process from Bi^{3+} to Eu^{3+} in $Gd_2O_3:Eu^{3+}$, Bi^{3+} (5 mol%) phosphor has been illustrated in the energy level scheme as presented in Fig. 11. Compared with UV light, phosphors emitting visible colour by the excitation of near-UV light around 365 nm are used in the fields of art and security, which wavelength is quite harmless to human bodies.

The thermoluminescence (TL) glow curves of 1 kGy gamma irradiated $Gd_2O_3:Eu^{3+}$, $Gd_2O_3:Eu^{3+}$, Bi^{3+} (1 mol%), $Gd_2O_3:Eu^{3+}$, Bi^{3+} (5 mol%) and $Gd_2O_3:Eu^{3+}$, Bi^{3+} (11 mol%) nanophosphors are shown in Fig. 12. All the samples were warmed at a heating rate of 20°C s^{-1}. A broad well-resolved TL glow peak at ∼380°C was observed in without Bi^{3+} co-doped $Gd_2O_3:Eu^{3+}$ samples (Fig. 12a). However, for the addition of Bi^{3+} (5 and 11 mol%) a shouldered peak (∼200°C) along with a well-resolved glow peak (∼380°C) was observed. This peak at 380°C is a dosimetrically useful peak and can be investigated further. The presence of a low-temperature peak around 200°C indicates that Bi co-doping favours formation of low-temperature traps.

It is observed that the TL intensity is found to be higher in $Gd_2O_3:Eu^{3+}$ samples when compared to Bi^{3+} co-doped $Gd_2O_3:Eu^{3+}$ sample. As the concentration of the Bi^{3+} ion impurity increases, it acts as a luminescent centre surrounded by the non-luminescent host centres. Therefore, the released charge carriers cannot recombine directly with the luminescent centres. The energy is transferred non-radiatively through the host lattice to the activator Bi^{3+}, which on recombination gives a characteristic emission. This may be due to the quenching effect of co-dopant concentration [29].

The kinetic (trapping) parameters such as activation energy (E), order of kinetics (b) and frequency factor (S) were

Table 1 The kinetic parameters estimated from Chen's glow peak shape method: (a) $Gd_2O_3{:}Eu^{3+}$, (b) $Gd_2O_3{:}Eu^{3+}$, Bi^{3+} (5 mol%) for 1 kGy gamma irradiation

Sample	T_m (°C)	μ_g (order of kinetics)	E_τ	E_δ	E_ω	E_{avg} (eV)	Frequency factor, S (s^{-1})
(a) $Gd_2O_3{:}Eu^{3+}$	380	0.41(1)	0.61	0.70	0.65	0.65	3.81×10^4
(b) $Gd_2O_3{:}Eu^{3+}$,	200	0.52(2)	0.90	0.92	0.91	0.91	4.30×10^9
Bi^{3+} (5 mol%)	366	0.51(2)	0.71	0.81	0.77	0.76	3.93×10^5

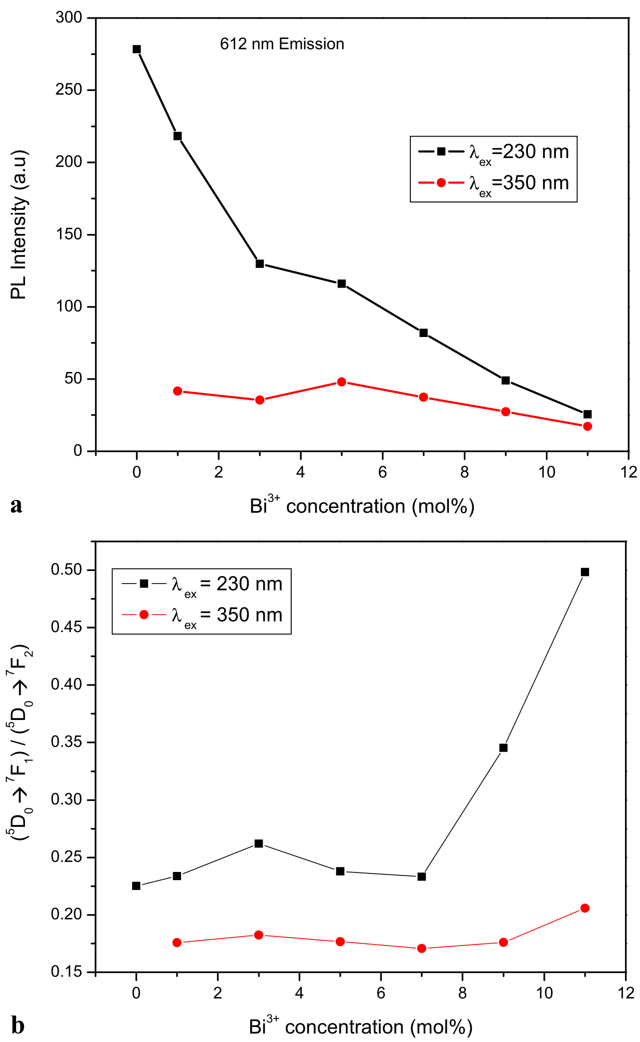

Fig. 10 (**a**) Variation in PL intensity of 612-nm emission peak versus Bi^{3+}concentration in $Gd_2O_3{:}Eu^{3+}$, Bi^{3+}. (**b**) Variation of ${}^5D_0 \rightarrow {}^7F_1/{}^5D_0 \rightarrow {}^7F_2$ ratio versus Bi^{3+} concentration in $Gd_2O_3{:}Eu^{3+}$, Bi^{3+} for 230 and 350 nm excitation wavelengths

estimated using Chen's set of empirical formulae [30] for the peak shape method as described below. The evaluated trapping parameters E and b were then used as the initial parameters in kinetic equations.

The activation energy E is given by

$$E_\alpha = c_\alpha\left(\frac{kT_m^2}{\alpha}\right) - b_\alpha(2kT_m), \tag{4}$$

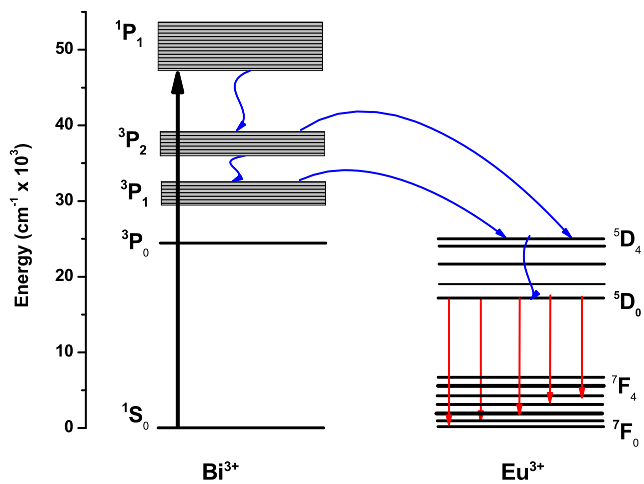

Fig. 11 The energy level scheme for the energy transfer from Bi^{3+} to Eu^{3+} ions

where $\alpha = \tau, \delta, \omega$ with $\tau = T_m - T_1, \delta = T_2 - T_m$, $\omega = T_2 - T_1$,

$$C_\tau = 1.51 + 3.0(\mu_g - 0.42),$$
$$b_\tau = 1.58 + 4.2(\mu_g - 0.42), \tag{5}$$

$$C_\delta = 0.976 + 7.3(\mu_g - 0.42), \qquad b_\delta = 0, \tag{6}$$

$$C_\omega = 2.52 + 10.2(\mu_g - 0.42), \qquad b_\omega = 1. \tag{7}$$

The geometrical form factor (symmetry factor) is given by

$$\mu_g = \frac{T_2 - T_m}{T_2 - T_1}. \tag{8}$$

The TL glow peak was deconvoluted using the Origin 8.0 software [31]. The estimated kinetic parameters for $Gd_2O_3{:}Eu^{3+}$ and Bi^{3+} (5 mol%) co-doped $Gd_2O_3{:}Eu^{3+}$ (4 mol%) nanophosphors are tabulated in Table 1.

4 Conclusions

Bi^{3+} co-doped $Gd_2O_3{:}Eu^{3+}$ (4 mol%) nanophosphors with monoclinic and little cubic phases were successfully synthesized by a low-temperature solution combustion process. The particle sizes was estimated using Scherrer's method and Williamson–Hall plots and were found to be in the

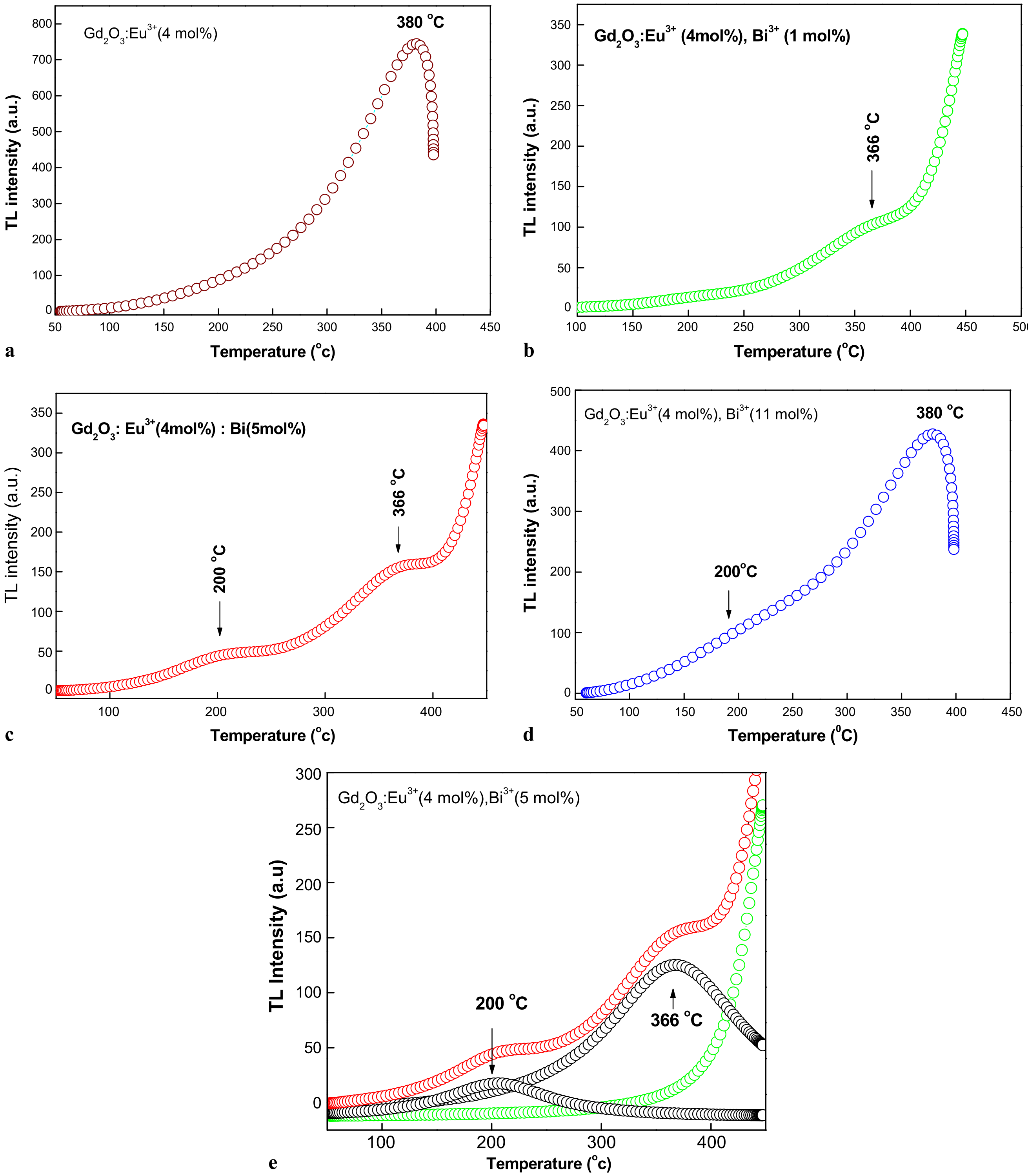

Fig. 12 TL spectra of Bi^{3+} co-doped Gd_2O_3:Eu^{3+}: (**a**) 0 mol%, (**b**) 1 mol%, (**c**) 5 mol%, (**d**) 11 mol%, (**e**) 5 mol% deconvoluted for 1 kGy gamma irradiation

ranges 40–60 nm and 30–80 nm, respectively. As the Bi^{3+} concentration increased, a shift in the excitation band to the longer-wavelength side was observed. The significant spectral overlap between the emission band of Bi^{3+} ions and the excitation band of Eu^{3+} ions resulted in efficient energy transfer from Bi^{3+} ions to Eu^{3+} ions. The energy transfer probability is strongly dependent upon the Bi^{3+} doping concentration. The optimum doping concentration was found to be 5 mol% of Bi^{3+} from fluorescence measurements. For higher concentrations of Bi^{3+} (>5 mol%), the absorbed energy was non-radiatively dissipated due to the formation of Bi^{3+} aggregates, which reduced the effectiveness of Bi^{3+} ions on sensitizing Eu^{3+} ions. The results of fluorescence intensity from Eu^{3+} and from Bi^{3+} due to energy transfer make $Gd_2O_3:Eu^{3+}$, Bi^{3+} nanophosphors, an attractive candidate for solid-state-lighting applications. From TL studies, a dosimetrically useful broad glow peak was observed at ~380°C in $Gd_2O_3:Eu^{3+}$ samples that can be investigated further.

Acknowledgements The authors are grateful to the TEQIP Chemistry Lab of M.S. Ramaiah Institute of Technology, Bangalore for providing facilities for preparation of materials. One of the authors (N.D.) acknowledges the Management, Principal and Head of Department, B.M.S. Institute of Technology, Bangalore for the support and encouragement.

References

1. C.R. Ronda, J. Lumin. **49**, 72 (1997)
2. G. Blasse, B.C. Grabmaier, *Luminescent Materials* (Springer, Berlin, 1994)
3. R.N. Bhargava, D. Gallagher, X. Hong, A.V. Nurmikko, Phys. Rev. Lett. **72**, 416 (1994)
4. H.S. Roh, Y.C. Kang, S.B. Park, J. Colloid Interface Sci. **228**, 195 (2000)
5. H. Yamamoto, SID J. **165**, 4 (1996)
6. T. Hirai, T. Orikoshi, J. Colloid Interface Sci. **269**, 103 (2004)
7. D. Dosev, I.M. Kennedy, M. Godlewski, I. Gryczynski, K. Tomsia, E.M. Goldys, Appl. Phys. Lett. **88**, 11906 (2006)
8. N. Dhananjaya, H. Nagabhushana, B.M. Nagabhushana, R.P.S. Chakradhar, C. Shivakumara, B. Rudraswamy, Physica B **405**, 3795 (2010)
9. B. Liu, M. Gu, X. Liu, C. Ni, D. Wang, L. Xiao, R. Zhang, J. Alloys Compd. **440**, 341 (2007)
10. S.H. Shin, J.H. Kang, D.Y. Jeon, D.S. Zang, J. Lumin. **114**, 275 (2005)
11. X. Liu, K. Han, M. Gu, L. Xiao, C. Ni, S. Huang, B. Liu, Solid State Commun. **142**, 680 (2007)
12. W.J. Park, M.K. Jung, S.J. Im, D.H. Yoon, Colloids Surf. A, Physicochem. Eng. Asp. **313**, 373 (2008)
13. Q. Xu, B. Lin, Y. Mao, J. Lumin. **128**, 1965 (2008)
14. L.G. Jacobsohn, B.C. Tappan, S.C. Tornga, M.W. Blair, E.P. Luther, B.A. Mason, B.L. Bennett, R.E. Muenchausen, Opt. Mater. **32**, 652 (2010)
15. N. Dhananjaya, H. Nagabhushana, B.M. Nagabhushana, B. Rudraswamy, C. Shivakumara, R.P.S. Chakradhar, J. Alloys Compd. **509**, 2368 (2011)
16. N. Dhananjaya, H. Nagabhushana, B.M. Nagabhushana, B. Rudraswamy, C. Shivakumara, R.P.S. Chakradhar, Physica B **406**, 1639 (2011)
17. X.T. Wei, Y.H. Chen, X.R. Cheng, M. Yin, W. Xu, Appl. Phys. B **99**, 763 (2010)
18. G. Blasse, B.C. Grabmaier, *Luminescent Materials* (Springer, Berlin, 1994), p. 55
19. Y. Porter-Chapman, E. Bourret-Courchesne, S.E. Derenzo, J. Lumin. **128**, 87 (2008)
20. D.R. Vij (ed.), *Thermoluminescent Materials* (PTR Prentice-Hall, Englewood Cliffs, 1993)
21. A.J.J. Bos, Nucl. Instrum. Methods B **184**, 3 (2001)
22. P. Klug, L.E. Alexander, *X-Ray Diffraction Procedures* (Wiley, New York, 1954)
23. G.K. Williamson, W.H. Hall, Acta Metall. **1**, 22 (1953)
24. H. You, M. Nogami, J. Phys. Chem. B **109**, 13980 (2005)
25. Z.F. Wang, W.P. Zhang, L. Lin, B.G. You, Y.B. Fu, M. Yin, Opt. Mater. **30**, 1484 (2008)
26. F. Real, V. Vallet, J.P. Flament, J. Schamps, J. Chem. Phys. **127**, 104705 (2007)
27. L.G. Jacobsohn, M.W. Blair, S.C. Tornga, L.O. Brown, B.L. Bennett, R.E. Muenchausen, J. Appl. Phys. **104**, 124303 (2008)
28. J. Tauc, in *Optical Properties of Solids*, ed. by F. Abeles (North-Holland, Amsterdam, 1970)
29. V. Kumar, R. Kumar, S.P. Lochab, N. Singh, Nucl. Instrum. Methods B **262**, 194 (2007)
30. R. Chen, J. Electrochem. Soc. **116**, 1254 (1969)
31. N. Dhananjaya, H. Nagabhushana, B.M. Nagabhushana, B. Rudraswamy, C. Shivakumara, K.P. Ramesh, R.P.S. Chakradhar, Physica B **406**, 1645 (2011)